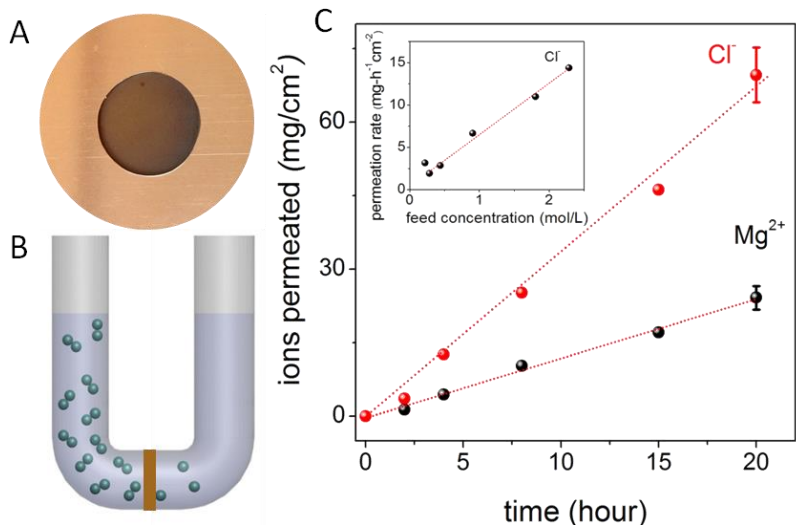




water. For a membrane with a thickness  $h$  of 1  $\mu\text{m}$ , we find water flow rates of  $\approx 0.2 \text{ L m}^{-2} \text{ h}^{-1}$  for 1 M feed solutions, and the speed increases with increasing the molar concentration  $C$ . Because 1 M corresponds to an osmotic pressure of  $\approx 25$  bar at room temperature, the flow rates agree with the evaporation rates of  $\approx 10 \text{ L m}^{-2} \text{ h}^{-1}$  reported for similar GO membranes, in which case the permeation was driven by a capillary pressure of the order of 1,000 bars (11).



*Fig. 1. Ion permeation through GO laminates. (A) Photograph of a GO membrane covering a 1 cm opening in a copper foil. (B) Schematic of the experimental setup. The membrane separates the feed and permeate containers (left and right, respectively). Magnetic stirring is used to ensure no concentration gradients. (C) Filtration through a 5  $\mu\text{m}$  thick GO membrane from the feed container with a 0.2 M solution of  $\text{MgCl}_2$ . The inset shows permeation rates as a function of  $C$  in the feed solution. Within our experimental accuracy (variations by a factor of  $<40\%$  for membranes prepared from different GO suspensions), chloride rates were found the same for  $\text{MgCl}_2$ ,  $\text{KCl}$  and  $\text{CuCl}_2$ . Dotted lines are linear fits.*

After establishing that GO membranes connect the feed and permeate containers with respect to transport of water molecules, we have investigated the possibility that dissolved ions and molecules can simultaneously diffuse through capillaries. To this end, we have filled the feed container with various solutions and studied if any of the solutes appears on the other side of GO membranes, that is, in the permeate container filled with deionized water (Fig. 1B). As a quick test, ion transport can be probed by monitoring electrical conductivity of water in the permeate container (Fig. S1). We have found that for some salts (for example,  $\text{KCl}$ ) the conductivity increases with time but remains unaffected for others (for example,  $\text{K}_3[\text{Fe}(\text{CN})_6]$ ) over many days of measurements. This suggests that only certain ions may diffuse through GO laminates. Note that ions are not dragged by the osmosis-driven water flow but move in the opposite direction.

To quantify permeation rates for diffusing solutes and test those that do not lead to an increase in conductivity (sucrose, glycerol and so on), we have employed various analytical techniques. Depending on a solute, we have used ion chromatography, inductively coupled plasma optical emission spectrometry, total organic carbon analysis and optical absorption spectroscopy (25). As an example, Figure 1C shows our results for  $\text{MgCl}_2$  which were obtained by using ion chromatography and inductively coupled plasma optical emission spectrometry for  $\text{Mg}^{2+}$  and  $\text{Cl}^-$ , respectively. One can see that concentrations of  $\text{Mg}^{2+}$  and  $\text{Cl}^-$  in the permeate container increase linearly with time, as expected. Slopes of such curves yield permeation rates. The inset of Fig. 1C illustrates that the observed rates depend linearly on  $C$  in the feed

container. Note that cations and anions move through membranes in stoichiometric amounts so that charge neutrality within each of the containers is preserved. Otherwise, an electric field would build up across the membrane, slowing fast ions until the neutrality is reached. In Fig. 1C, permeation of one  $\text{Mg}^{2+}$  ion is accompanied by two ions of chloride, and the neutrality condition is satisfied.

Figure 2 summarizes our results obtained for different ionic and molecular solutions. The small species permeate with approximately the same speed whereas large ions and organic molecules exhibit no detectable permeation. The effective volume occupied by an ion in water is characterized by its hydrated radius. If plotted as a function of this parameter, our data are well described by a single-valued function with a sharp cutoff at  $\approx 4.5\text{\AA}$  (Fig. 2). Species larger than this are sieved out. This behavior corresponds to a physical size of the mesh of  $\approx 9\text{\AA}$ . Fig. 2 also shows that permeation rates do not exhibit any notable dependence on ion charge (12,13,23,26) and triply charged ions such as  $\text{AsO}_4^{3-}$  permeate with approximately the same rate as singly-charged  $\text{Na}^+$  or  $\text{Cl}^-$ . Finally, to prove the essential role of water for ion permeation through GO laminates, we dissolved  $\text{KCl}$  and  $\text{CuSO}_4$  in DMSO, the polar nature of which allows solubility of these salts. No permeation has been detected, proving that the special affinity of GO laminates to water is important.

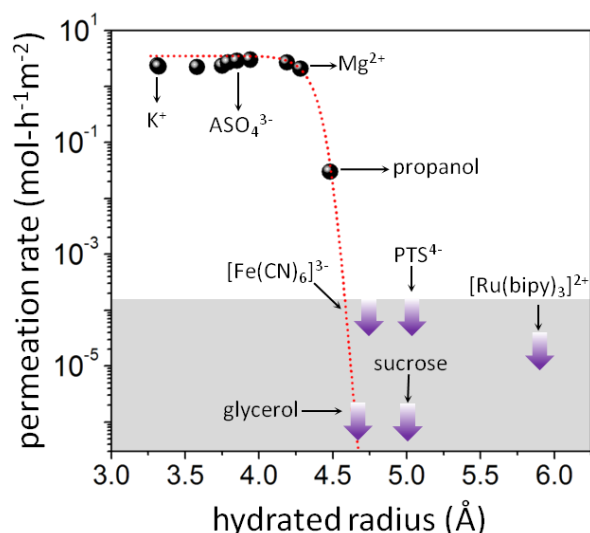
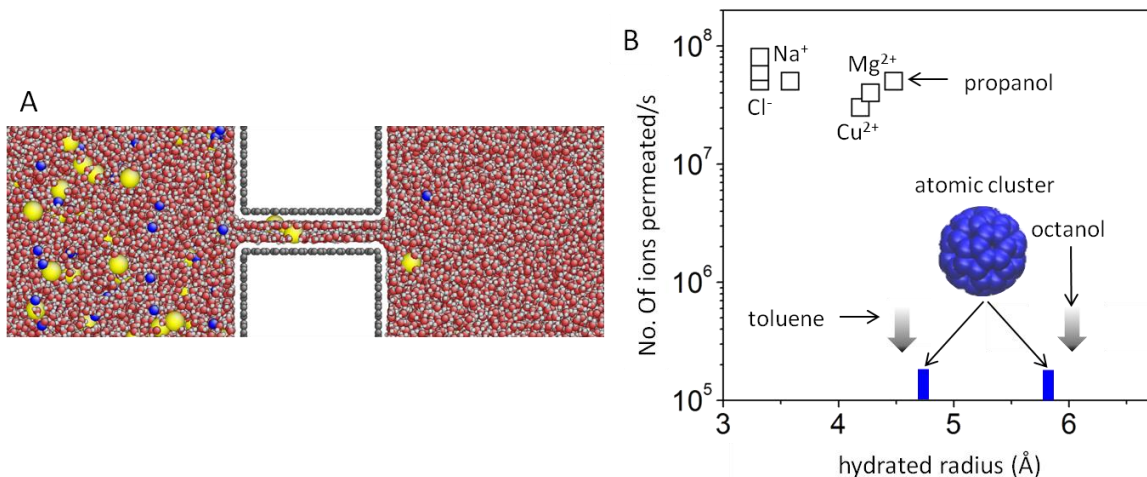


Fig. 2. Sieving through an atomic scale mesh. The shown permeation rates are normalized per 1M feed solution and measured by using  $5\ \mu\text{m}$  thick membranes. Some of the tested chemicals are named here; the others can be found in Table S1 (25). No permeation could be detected for the solutes shown within the grey area during measurements lasting for 10 days or longer. The thick arrows indicate our detection limit that depends on a solute. Several other large molecules including benzoic acid, DMSO and toluene were also tested and exhibited no detectable permeation. The dashed curve is a guide to the eye, showing an exponentially sharp cutoff with a semi-width of  $\approx 0.1\text{\AA}$ .

To explain the observed sieving properties, we employ the model previously suggested to account for unimpeded evaporation of water through GO membranes (11). Individual GO crystallites have two types of regions: functionalized (oxidized) and pristine (21,27,28). The former regions act as spacers that keep adjacent crystallites apart. In a hydrated state, the spacers help water to intercalate between GO sheets, whereas the pristine regions provide a network of capillaries that allow nearly frictionless flow of a layer of correlated water, similar to the case of water transport through carbon nanotubes (8-10). The earlier experiments using GO laminates in air with a typical  $d \approx 10\ \text{\AA}$  have been explained by assuming one monolayer of moving water. For GO laminates soaked in water,  $d$  increases to  $\approx 13 \pm 1\ \text{\AA}$ , which allows two or three monolayers (19,22,23,29). Taking into account the effective thickness of graphene of  $3.4\ \text{\AA}$

(interlayer distance in graphite), this yields a pore size of  $\approx 9\text{-}10$  Å, in agreement with the mesh size found experimentally.



*Fig. 3. Simulations of molecular sieving. (A) Snapshot of NaCl diffusion through a 9 Å graphene slit allowing two monolayers of water. Na<sup>+</sup> and Cl<sup>-</sup> ions are in yellow and blue, respectively. (B) Permeation rates for NaCl, CuCl<sub>2</sub>, MgCl<sub>2</sub>, propanol, toluene and octanol for capillaries containing two monolayers of water. For octanol poorly dissolved in water, the hydrated radius is not known and we use its molecular radius. Blue marks: Permeation cutoff for an atomic cluster (pictured in the inset) for capillaries accommodating two and three monolayers of water (width of 9 Å and 13 Å, respectively).*

To support our model, we have used molecular dynamics simulations (MDS). The setup is shown in Fig. 3A where a graphene capillary separates feed and permeate reservoirs, and its width is varied between 7 and 13 Å to account for the possibility of one, two or three monolayers of water (25). We find that the narrowest MDS capillaries become filled with a monolayer of ice as described previously (11) and do not allow inside even such small ions as Na<sup>+</sup> and Cl<sup>-</sup>. However, for two and three monolayers expected in the fully hydrated state, ions enter the capillaries and diffuse into the permeate reservoir. Their permeation rates are found approximately the same for all small ions and show little dependence on ionic charge (Fig. 3B). Larger species (toluene and octanol) cannot permeate even through capillaries containing three monolayers of water (Fig. S3). We have also modeled large solutes as atomic clusters of different size (25) and found that the capillaries accommodating 2 and 3 water monolayers rejects clusters with the radius larger than  $\approx 4.7$  and  $5.8$  Å, respectively. This probably indicates that the ion permeation through GO laminates is limited by regions containing two monolayers of water. The experimental and theory results in Figs 2 & 3B show good agreement.

Now we turn our attention to the absolute value of ion permeation rates found experimentally. Following ref. 11, one can estimate that, for our laminates with  $h \approx 5$  μm and  $L \approx 1$  μm, the effective length of graphene capillaries is  $L \times h/d \approx 5$  mm and they occupy  $d/L \approx 0.1\%$  of the surface area of the GO membrane. Accordingly, for a typical diffusion coefficient of ions in water ( $\approx 10^{-5}$  cm<sup>2</sup>/s), we expect permeation rates thousands times smaller than those found experimentally. Moreover, this estimate neglects the fact that functionalized regions narrow the effective water column (11). To appreciate how fast the observed permeation is, we have used the standard coffee filter paper and found the same diffusion rates for the paper of 1 mm in thickness (the diffusion barrier is equivalent to a couple of mm of pure water). Such fast transport of small ions cannot be explained by the confinement, which increases the diffusion coefficient by 50%, reflecting the change from bulk to two-dimensional water (25). Furthermore, functionalized regions [modeled as graphene with randomly attached epoxy groups (20,21)] do not enhance diffusion but rather suppress it (25,29) as expected because of the broken translational symmetry.

To understand the ultrafast ion permeation, we recall that graphene and GO powders exhibit a high adsorption efficiency with respect to many salts (30). Despite being very densely stacked, GO laminates are found to retain this property for salts with small hydrated radii [section 5 of (25)]. Our experiments show that permeating salts are adsorbed in amounts reaching as much as 25% of membranes' initial weight (*Fig. S2*). The large intake implies highly concentrated solutions inside graphene capillaries (close to the saturation). Our MDS simulations confirm that small ions prefer to reside inside capillaries (*Fig. S4*). The affinity of salts to graphene capillaries indicates an energy gain with respect to the bulk water, and this translates into a capillary-like pressure that acts on ions within a water medium, rather than on water molecules in the standard capillary physics (25). Therefore, in addition to the normal diffusion, there is a large capillary force, sucking small ions inside the membranes and facilitating their permeation. Our MDS provide an estimate for this ionic pressure as  $\approx 50$  bars (25).

The reported GO membranes exhibit extraordinary separation properties and their full understanding will require further work both experimental and theoretical. In particular, it remains unclear whether the functionalized regions play any other significant role, except for being spacers. In fact, the regions are negatively charged in water and may further enhance the ion sponge effect with respect to pristine graphene capillaries. With the ultrafast ion transport and atomic-scale pores, GO membranes present an interesting material to consider for separation and filtration technologies, particularly, those that target extraction of valuable solutes from complex mixtures.

1. K. B. Jirage, J. C. Hulteen, C. R. Martin. *Science* **278**, 655 (1997).
2. N.B. McKeown, P. Budd. *Chem. Soc. Rev.* **35**, 675 (2006).
3. D. L. Gin, R. D. Noble. *Science* **332**, 674 (2011).
4. D. Cohen-Tanugi, J. C. Grossman. *Nano Lett.* **12**, 3602 (2012).
5. S. P. Koenig, L. Wang, J. Pellegrino, J. S. Bunch. *Nat. Nanotechnol.* **7**, 728(2012).
6. M. Ulbricht. *Polymer* **47**, 2217 (2006).
7. M. Elimelech, W. A. Phillip. *Science* **333**, 712 (2011).
8. J. K. Holt *et al.* *Science* **312**, 1034 (2006).
9. M. Majumder, N. Chopra, R. Andrews, B. J. Hinds. *Nature* **438**, 44 (2005).
10. G. Hummer, J. C. Rasaiah, J. P. Noworyta. *Nature* **414**, 188 (2001).
11. R. R. Nair *et al.* *Science* **335**, 442 (2012).
12. M. Majumder, N. Chopra, B. J. Hinds. *J. Am. Chem. Soc.* **127**, 9062 (2005).
13. F. Fornasiero *et al.* *Proc. Natl. Acad. Sci. U. S. A* **105**, 17250 (2008).
14. L. Qiu *et al.* *Chem. Comm.* **47**, 5810 (2011).
15. P. Sun *et al.* *ACS Nano* **7**, 428 (2013).
16. Y. Han, Z. Xu, C. Gao. *Adv. Funct. Mater.* **23**, 3693 (2013).
17. M. Hu, B. Mi. *Environ. Sci. Technol.* **47**, 3715 (2013).
18. H. Huang *et al.* *Chem. Comm.* **49**, 5963 (2013).
19. K. Raidongia, J. Huang. *J. Am. Chem. Soc.* **134**, 16528 (2012).
20. D. A. Dikin *et al.* *Nature* **448**, 457 (2007).
21. G. Eda, M. Chhowalla. *Adv. Mater.* **22**, 2392 (2010).
22. A. Lerf *et al.* *J. Phys. Chem. Solids* **67**, 1106 (2006).
23. D. W. Boukhvalov, M. I. Katsnelson, Y.-W. Son. *Nano Lett.* **13**, 3930 (2013).
24. S. You, S. M. Luzan, T. Szabo, A. V. Taluzin. *Carbon* **52**, 171 (2013).
25. See supporting materials.
26. B. Van der Bruggen, J. Schaep, D. Wilms, C. Vandecasteele. *J. Membr. Sci.* **156**, 29 (1999).
27. N. R. Wilson *et al.* *ACS Nano* **3**, 2547 (2009).
28. D. Pacile *et al.* *Carbon* **49**, 966 (2011).
29. N. Wei, Z. Xu. arXiv:1308.5367.
30. S. Wang, H. Sun, H. M. Ang, M. O. Tade. *Chem. Eng. J.* **226**, 336 (2013).